UTILIZATION OF GASES FROM BIOMASS GASIFICATION IN A REFORMING REACTOR COUPLED TO AN INTEGRATED PLANAR SOLID OXIDE FUEL CELL: SIMULATION ANALYSIS

by

Paola COSTAMAGNA, Fabio CERUTTI, Renzo Di FELICE, and Robert COLLINS

Original scientific paper
UDC: 662.636/.638
BIBLID: 0354-9836, *8* (2004), 2, 127-142

One of the high-efficiency options currently under study for a rational employment of hydrogen are fuel cells. In this scenario, the integrated planar solid oxide fuel cell is a new concept recently proposed by Rolls-Royce. The basic unit of a modular plant is the so called "strip", containing an electrochemical reactor formed by a number of IP-SOFC modules, and a reforming reactor. For a better understanding of the behaviour of a system of this kind, a simulation model has been set up for both the electrochemical reactor and the reformer; both models follow the approach typically employed in the simulation of chemical reactors, based on the solution of mass and energy balances. In the case of the IP-SOFC electrochemical reactor, the model includes the calculation of the electrical resistance of the stack (that is essentially due to ohmic losses, activation polarisation and mass transport limitations), the mass balances of the gaseous flows, the energy balances of gaseous flows (anodic and cathodic) and of the solid. The strip is designed in such a way that the reaction in the reforming reactor is thermally sustained by the sensible heat of the hot air exiting the electrochemical section; this heat exchange is taken into account in the model of the reformer, which includes the energy balance of gaseous flows and of the solid structure.
Simulation results are reported and discussed for both the electrochemical reactor in stand-alone configuration (including comparison to experimental data in a narrow range of operating conditions) and for the complete strip.

Key words: *hydrogen, chemical reactor, fuel cell, reformer, modelling*

Introduction

The European Union are strongly committed at scientific, technological and, last but not least, political levels to implement and widen the utilization of hydrogen as innovative energy vector, either in stationary applications of large and small scale (among these, the distributed and combined generation of electric power and heat), and for transport.

When focussing on issues related to hydrogen production, it has to be stressed that the question is not about hydrogen availability (it has been estimated that less than a quarter of hydrogen today produced in oil refineries and petrochemical plants around Europe would be enough to fuel 5% of all cars in this continent); the question is how to produce hydrogen in a sustainable way, *i. e.* without utilizing fossil energy sources, as it happens today, which pose the problem of accumulation of greenhouse gases in the atmosphere, in addition to the well known "weaknesses" related to the supply from politically turbulent geographical sites.

A route which is unanimously considered very promising is the utilization of renewable sources, specifically biomass feedstock. Among the biomass conversion processes, steam gasification has been already validated by means of practical applications and has shown itself to be appropriate to the goal of hydrogen production [1].

In this paper, however, we consider the successive step: how a typical gaseous stream produced from biomass can be efficiently used from an energy point of view after the cleaning process has taken place. For sake of simplicity, we have assumed the biogas to be represented by methane in all the simulations of the strip, which is the basic unit of the IP-SOFC modular plant.

Description of the electrochemical reactor, reformer, and strip

The integrated planar solid oxide fuel cell (IP-SOFC) is a new concept recently proposed by Rolls-Royce, which is substantially a cross between the traditional tubular and planar SOFC geometries [2, 3], seeking to borrow thermal expansion tolerance from the former and low cost component fabrication and short current paths from the latter. The scheme reported on the left-hand side of fig.1 clearly shows the sequence of the various components in each single cell of the IP-SOFC concept; the thickness of the electrodes and the electrolyte is about 20-30 m each. The electrochemical reactions are:

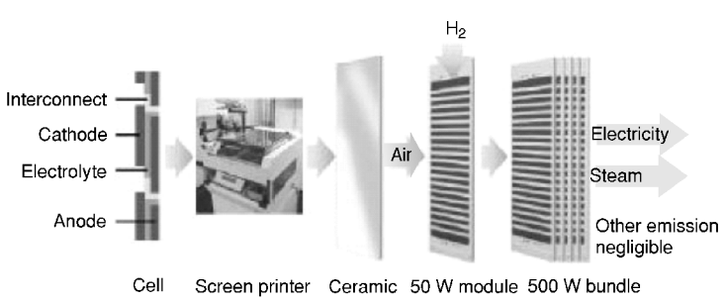

Figure 1. Scheme of the multi-cell MEA concept (left); module and bundle configuration (right)

$$H_2 + O^{--} \rightarrow H_2O + 2e^- \qquad \text{anode} \qquad (1)$$

$$CO + O^{--} \rightarrow CO_2 + 2e^- \qquad \text{anode} \qquad (2)$$

$$O_2 + 4e^- \rightarrow 2O^{--} \qquad \text{cathode} \qquad (3)$$

There are also chemical reactions occurring at the anodic side when CH_4, CO, and H_2O are present in the fuel flow:

$$CH_4 + H_2O \rightarrow CO + 3H_2 \qquad \text{reforming} \qquad (4)$$

$$CO + H_2O \rightarrow CO_2 + H_2 \qquad \text{shifting} \qquad (5)$$

In order to obtain high voltages and low electrical currents, several cells of small dimensions are deposited over a vertical porous ceramic support (fig.1, middle) and electrically connected in series, forming the so-called *multi-cell module* (fig.1, middle), where the cells appear as small stripes; the module is fed externally with air and internally with fuel (through channels located inside the support). A cross section of the module, showing the details of the fuel channels, is depicted in fig. 2 for two different module geometries, *i. e.* the 1-C geometry (currently under study for application in the plant configurations described below) and the 3-C geometry, used for experimentation purposes. In the 3-C geometry, fuel is fed into the inner channel where, if the fuel contains methane and water, reforming reaction can occur. Then, the flows gets divided into two parts (at the top of the module) and enters the two anodic channels. The air flow is in counter-current with anodic gas. In the 1-C geometry, which is simpler than the 3-C one, fuel flows

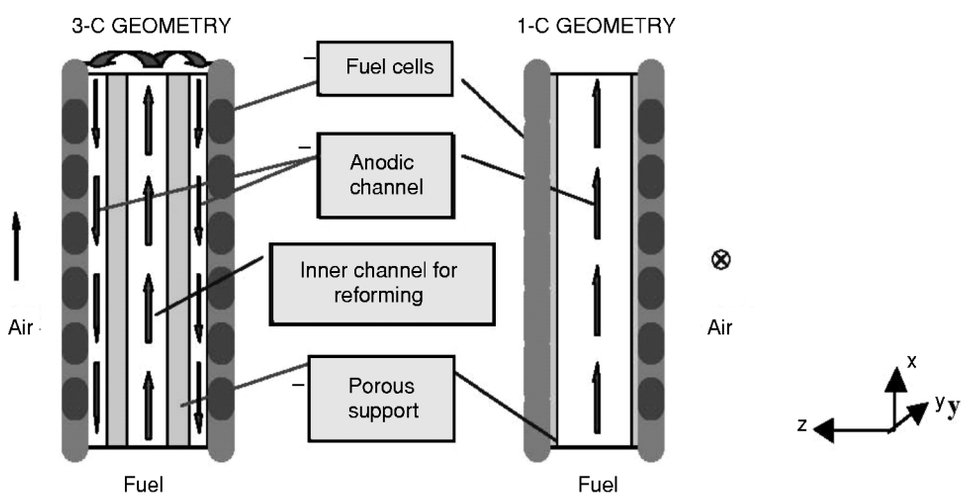

Figure 2. Flow distribution in 3-C and 1-C modules

through the only internal anodic channel and air flows in the perpendicular direction. In both cases, each module is double-sided by depositing an identical series of multi-cells on both sides of a porous support; in this paper the attention is focused on modules with 20 cells per side. Additional details about the geometric arrangement are reported in [10].

Modules (1-C geometry) are then grouped in bundles (right-hand side of fig. 1), the electrochemical bundle being composed of a number of modules in electrical series with each other; from the gas distribution point of view, the fuel flows in series along the modules composing the bundle, while air flows in parallel through all of them. Then, a strip (fig. 3) is composed by a number of electrochemical bundles coupled to a reformer where the catalytic reforming of methane occurs to produce a fuel gas rich in H_2 and CO to be fed into the fuel cells. The structure of the reforming bundle is very similar to that of the electrochemical bundle: for example, it is usually composed by a number of reforming modules. The basic difference between the two types of bundles is that the reforming modules have no electrochemical cells but instead contain a reforming catalyst system. Wit hin the strip , the elec- tro- che mi- cal bun- dles are in elec- tri- cal se- ries each othe r.

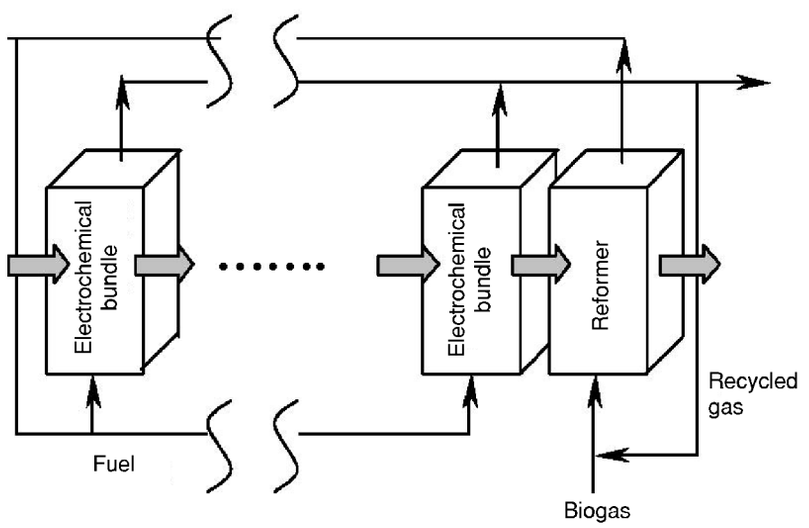

Figure 3. Scheme of the strip configuration

Concerning flow distribution, the electrochemical bundles are fed in parallel by the fuel gas produced by reformer, while the air flow crosses the bundles one after the other, *i. e*. in series. After flowing through the last electrochemical bundle, the air is fed into the reforming bundle, where it provides the heat necessary for the reforming endothermic reaction. As far as the gas to be reformed is concerned, preheated methane is mixed with a part of the water-rich, high temperature exhaust fuel recycled from the outlet of the electrochemical bundles.

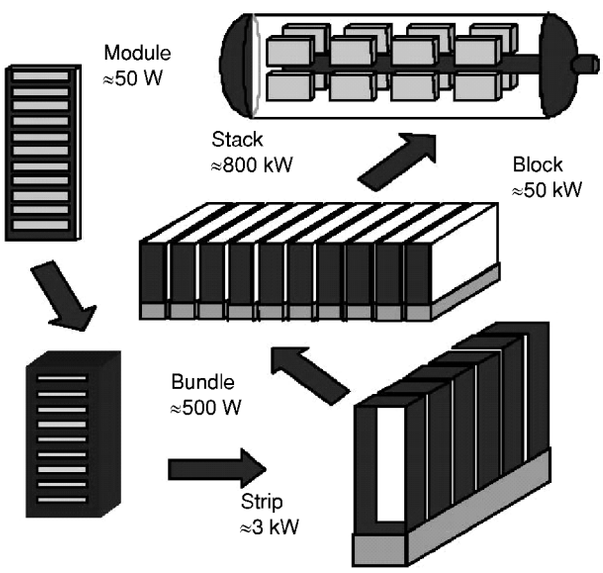

Figure 4. Scale-up from module to stack

Finally, several strips form a block, which is an essential part of a hybrid plant (fig. 4), which combines this technology together with a gas turbine in order to provide a high efficiency power generation system. Such systems are the focus of current research within a project supported by the European Union (more details are reported in the section "Acknowledgments"). The goal of the present study was to develop a suitable model of the strip, which could then be integrated in a system simulation tool designed to support thermodynamic analysis of hybrid IP-SOFC/GT (gas turbine) systems [4].

Simulation model

Model of the electrochemical reactor

Several models have been proposed in the literature for the steady-state and transient simulation of various SOFC concepts (for example, see [5-9]). Here, a one-dimensional, steady state model of an IP-SOFC single module and bundle has been developed, under the hypothesis reported in tab. 1.

The module is modelled as a sequence of cells electrically connected in series; the model includes a detailed evaluation of the local electrochemical kinetics of the reactor, based on the evaluation of the local Nernst's voltage and of ohmic, activation and concentration losses. For a given current, the model of the electrochemical kinetics allows to calculate the average voltage of each cell of the module. Further details about this model are given in [10], which also shows a validation of the electrochemical kinetics

Table 1. Modelling Hypothesis

• One-dimensional model along the x co-ordinate displayed in fig. 2
• Fuel: pre-reformed methane (CH_4, CO_2, CO, H_2, H_2O), oxidant, air
• Shifting and reforming reactions are assumed to be at equilibrium within the anodic flow
• Same electrical current for all the cells of the module
• No heat exchange by radiation between gases and solid
• No heat exchange between module and environment
• Plug-flow form for mass and energy balances

model, based on experimental results collected from small scale experimental single cells. All the electrochemical properties and electrical conductivities have been taken from the literature [11]. When the model of the electrochemical kinetics is included into the overall model of the module, an additional type of resistance is taken into consideration, *i. e.* the contact resistance (an approach used in other literature papers about fuel cell simulation, see for example [9]). This type of resistance in principle takes into account the fact that a full size stack is usually affected by small defects, *i. e*. pinholes, delamination, *etc*., which affect negatively the performance, and thus the performance which is not simply proportional to the performance of small scale experimental single cells. The contact resistance is assumed to be constant (0.077), *i. e*. completely independent of the operating conditions of temperature, concentration, *etc.*

In addition to the local electrochemical kinetics, the model of the module includes mass and energy balances (tab. 2). In particular, mass balances (eq. 6) allow the evaluation of the gaseous flow compositions over the fuel cell module taking into account the consumption and production rates due to the electrochemical (1-3) and chemical (4, 5) reactions. The energy balances of the gaseous flows allow the evaluation of the temperature of the reactant gases, which varies along the flow direction due to gas-solid heat transfer due to mass transfer (second term in eq. 7), and convective heat exchange between solid walls and bulk of gases (third term in eq. 7); B_g is the ratio between the gas-solid effective heat-exchange area and the cell area, and h_g is the heat transfer coefficient calculated from the Nusselt number for laminar flow (eq. 10). The solid energy balance (eq. 8) takes into account, in order, the forced convective gas-solid heat exchange, the heat dissipation due to the electrochemical reaction and the heat conduction within the solid structure; the solid thermal conductivity K_x is evaluated considering the layered structure (eq. 9), where δ_h is the thickness of a single layer.

The system of equations is integrated numerically through a Fortran program, using a finite difference method (eqs. 6-7) to a relaxation method for eq. 8. Indeed, the module can be simulated under either isothermal conditions (by excluding eq. 8 from the numerical integration and using a predefined field of temperatures) or adiabatic condi-

Table 2. Basic equations of the model of the electrochemical module

- Local kinetics: electro-kinetics + equilibrium of shifting and reforming

- Mass and energy balances of the gaseous streams

  Mass balance: $\frac{\partial n_i}{\partial x} \quad r_i$ (6)

  Energy balance: $\quad n_i c_{p,i} \frac{\partial T_g}{\partial x} \quad \quad c_{p,i} \frac{\partial n_i}{\partial x}(T_g \quad T_s) \quad hB \frac{1}{a}(T_g \quad T_s) \quad 0$ (7)

- Energy balance of the solid

  $\frac{1}{s} \quad hB(T_g \quad T_s) \quad \frac{1}{s} \frac{\Delta H}{n_e \mathrm{F}} \quad V \quad I \quad K_x \frac{\partial^2 T_s}{\partial x^2} \quad 0$ (8)

  $K_x \quad \frac{K_h \delta_h}{\delta_h}$ (9)

  $h \quad \frac{\mathrm{Nu}\,\lambda}{d_h}$ (10)

tions (in this case, eq. 8 is used to evaluate the temperature profile). In the isothermal case, it is possible to simulate the electrochemical performance (in terms of I-V curves) at different imposed operational temperatures; the option of running the simulation with isothermal solid temperature distribution is often applied, since this is the condition under which some experimental data are obtained at Rolls-Royce Fuel Cells Systems Ltd. (see fig. 7) All the other results reported in this paper have been obtained under adiabatic conditions (*i. e*. perfect insulation of the vessel where the module is contained), since this is a realistic practical operating condition for the module when included into the plant.

Finally, the electrochemical bundle is simulated, with a good degree of approximation, as a long module with a number of cells per side equal to the number of cells per side of one module times the number of modules in the bundle. No heat exchange by convection or radiation between the different modules of the bundle is yet considered.

Model of the reforming reactor

The reforming bundle has been simulated, as the electrochemical one, as a long module, with a length equal to the length of a single module times the number of modules in the bundle. The model is 1-D, and no heat exchange by convection, radiation or conduction between the different modules of the bundle has been considered. The reforming reaction is considered to be coupled to the shifting reaction; shifting is considered at equilibrium, and reforming, in the present version of the model, is simulated supposing

that, at the outlet of each single reforming cell, $\prod_i p_i^{\nu_i}$ is equal to 0.1 the equilibrium constant. This is a preliminary and approximated way of taking the reforming kinetics into account. Mass and energy balances of the gaseous flows have been included, as well as the energy balances for the solid structure, written in the same form used for the electrochemical reactor (eqs. 6-10).

Strip model

The model of the strip has been developed coupling between them the 1-D models of the electrochemical and the reforming bundles, taking into account the flow scheme reported in fig. 3.

Results and discussion

Electrochemical reactor

Figures below report some simulation results obtained for a module with 1-C geometry, having cells per side and operated under the conditions given in tab. 3.

Table 3. Operating conditions for the simulation of the IP-SOFC module

Fuel flowrate 4.3 Nl/min.
Air flowrate 25 Nl/min.
Molar fuel composition 50% H_2, 18% H_2O, 2% CH_4, 10% CO_2, 20% CO
Fuel inlet temperature 800 °C
Air inlet temperature 800 °C
Current density 280 mA/cm^2
Pressure 1 atm

Figure 5a shows the solid temperature distribution along the x co-ordinate of the module. The abscissa of the plot indicates the cell numbers along the module (cells are numbered from bottom to top, so that cell no. 1 is the cell located at the bottom of the module, where fresh fuel is introduced).

Figure 5a shows that solid temperature increases from bottom to top due to the heat dissipated by the electrochemical reaction. The voltage distribution along the module follows quite faithfully the solid temperature distribution, as reported in fig. 5b, and this is mainly due to the fact that voltage losses (reported in fig. 5b decrease with increasing temperature. Furthermore, fig. 6a reports the behaviour of all the different types of overpotentials along the module; apart from contact resistance which, as already discussed, assumes a constant value, all the other overpotentials decrease along the module

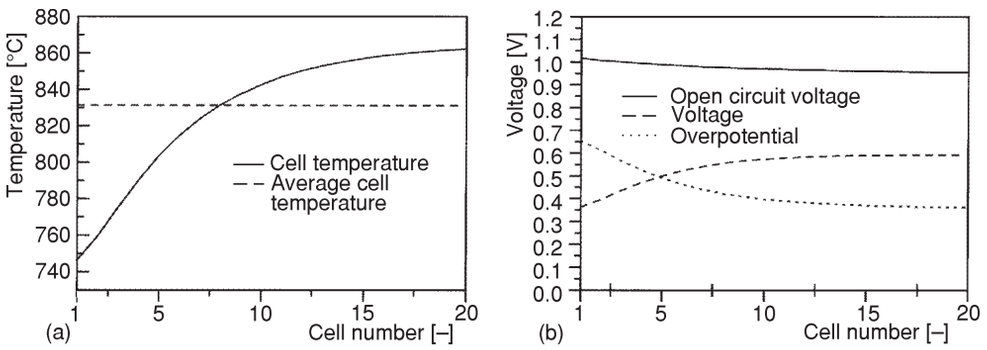

Figure 5. Distribution of temperature and voltage in a 20-cell module

due to the increase of solid temperature [10]. Finally, in fig. 6b, the distribution of the concentrations within the anodic gases is reported as a function of the x co-ordinate. Indeed, at the bottom of the module, H_2 concentration increases and H_2O decreases due to the reforming reaction which is faster than the electrochemical one. After only a couple of cells, CH_4 is almost totally consumed so that from this point the only effects are due to H_2 consumption and H_2O production due to the electrochemical reaction (since the equilibrium of shifting reaction is included in the simulation as well, it has some effects, in particular on the CO concentration).

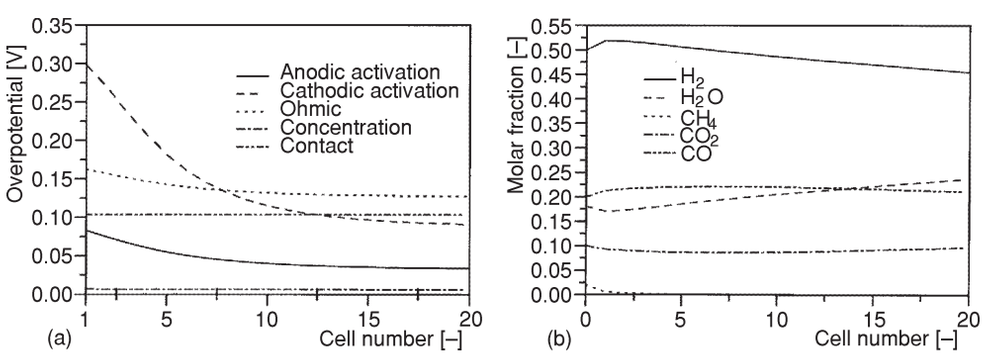

Figure 6. Distribution of voltage losses and fuel compositions in a 20-cell module

The modelling results have also been compared against experimental data obtained from a 3-C experimental module operated into a muffle furnace kept at 950 C, modified to enable fuel and air to be fed to the test module, and to allow electrical mea-

surements to be made. The experimental apparatus has been designed, built and operated by Rolls-Royce Fuel Cell Systems Ltd.

Characteristic V-I curves were measured at atmospheric pressure with different fuel flows of $H_2/H_2O/CO/CO_2$ mixtures and with air used as the oxidant. Under these operating conditions, the module is considered to be isothermal in all the simulation, since, due to the effective radiation between the module and the muffle, the module temperature is expected to have a temperature very close to that of the muffle itself. A comparison between experimental and simulation results is reported in fig. 7, which compares three V-I curves obtained with a fuel flow of 10 Nl/min. and different fuel compositions (Case 1: 19% CH_4, 54% H_2, 27% CO; Case 2: 1.4% CH_4, 65.6% H_2, 33% CO; Case 3: 66.7% H_2, 18.7% CO, 14.6% CO_2; compositions reported here are dry compositions, and fuel is humidified at ambient temperature before been fed into the experimental module). Figure 7 reports a very good agreement between simulated and experimental results, and in particular a peculiar trend displayed by the experimental data is very well followed by the simulation, *i. e*. the fact that the lower the hydrogen content in the fuel, the higher the performance.

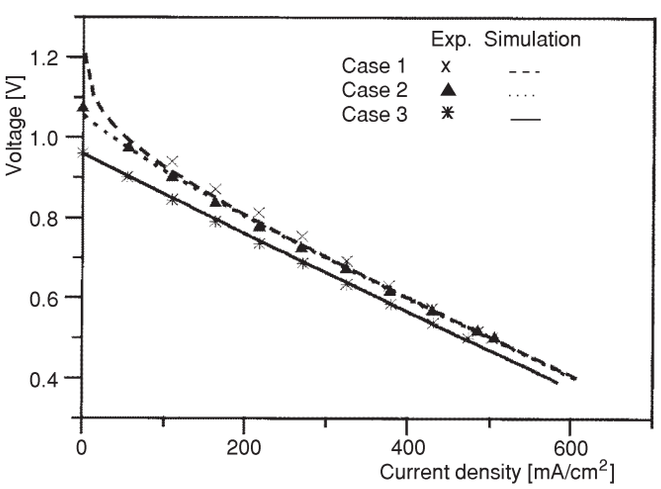

Figure 7. Comparison between modelling results and experimental data for the 3-C electrochemical module 950 °C

This behaviour may be explained if one considers the water content of the fuel mixtures rather than the hydrogen content. Mixture 2 contains only hydrogen, carbon monoxide and water. This mixture will not react further on either the anodes or the support. Mixture 3 however contains some 14.6% carbon dioxide. At such high temperatures this mixture is fully expected to undergo the water gas shift reaction on both the anodes and the porous ceramic support. Thermodynamic calculations indicate that at 950 °C

mixture 3 will shift to produce an equilibrium mixture containing 55.5% H_2, 12.2% H_2O, 5.4% CO_2, 26.8% CO, and 0.1% CH_4. Compared with mixture 2 it is now obvious why mixture three gives poorer performance despite having a slightly higher initial hydrogen content.

If mixture 1 is now considered it can be seen the it contains 19% methane but only approximately 3% water. The methane and water are expected to react on the fuel cell anodes via the steam reforming reaction. The large excess of methane will result in almost complete depletion of the water content of the fuel gas. It is this depletion of the water content and not the hydrogen concentration that leads an increase in the Nernst voltage and hence to improved performance of the fuel cells.

Thus, a correct simulation of the reforming and shifting reactions is essential in order to be able to predict the experimental performance under these operating conditions; the good agreement between the experimental and simulation results confirms that equilibrium (tab. 1) is a good assumption for the reforming and shifting reactions.

Strip

Some results are reported below for an IP-SOFC strip composed by 5 electrochemical bundles, each composed of 7 modules with 20 cells per side; the reformer is composed by 4 reforming modules of equivalent 14 cell length. The operating conditions are summarised in tab. 4.

Table 4. operating conditions for the strip

Methane flow rate 4.38 Nl/min.
Air flow rate 262.5 Nl/min.
Methane inlet temperature 510 °C
Air inlet temperature 808 °C
Current density 280 mA/cm^2
Contact resistance 0 ohm
Recycling ratio 6.5 kg/kgCH_4
Pressure 7 atm

The results obtained are reported in figs. 8 and 9. In particular, fig. 8 displays the compositions of the fuel flow at different points of the strip (note that the H_2O/CH_4 ratio is always above 2.2, which guarantees that no carbon deposition takes place), as well as the temperatures in the most critical parts of the strip itself. The results demonstrate that temperature is within the acceptable values for SOFCs, and thus the feasibility of the concept. The total power supplied is 1.49 kW and the efficiency is 57.1% (the efficiency being defined as the ratio between the output electrical power and the lower heating vlaue of the inlet methane).

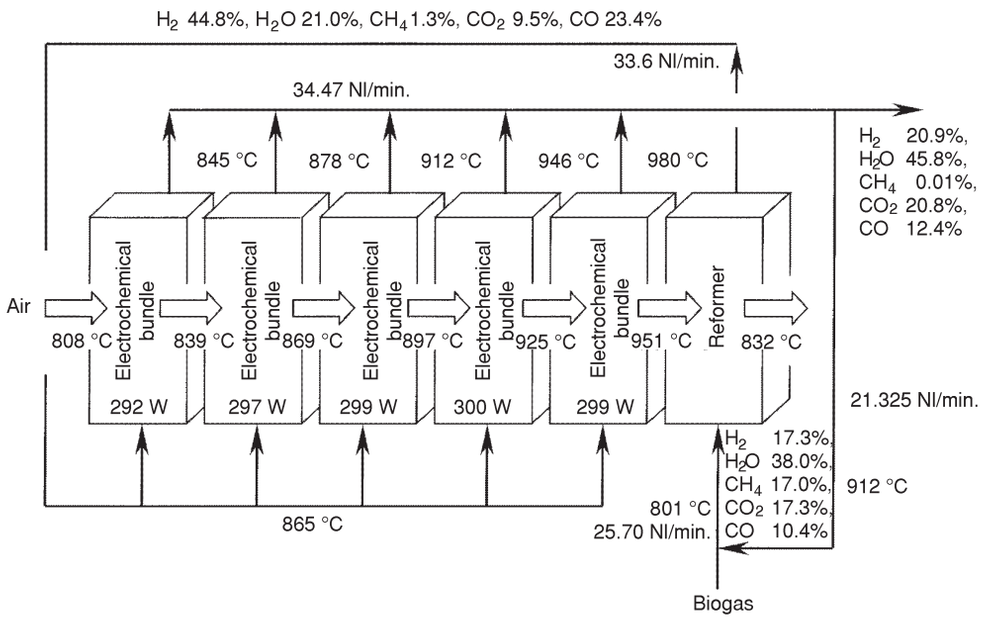

Figure 8. Results for the simulated strip

Figure 9a reports the details of the distribution of solid, fuel and air temperature profiles (air temperature is the temperature of the air at the outlet of each cell of the bundle). Because of the high heat exchange coefficient between gases and solid, fuel and outlet air and solid temperature profiles are very close to each other. In each of the bundles, solid temperature changes occur mainly in the first twenty cells (*i. e.* first module), which are then subject to the most severe thermal gradient and material stresses. Temperature increases from the first to the last bundle: in fact, since bundles are crossed in series by the air (while inlet fuel flow rate and temperature, as well as current densities are the same for all the bundles), the exit temperature of air from a bundle is the same as the inlet temperature of air into the subsequent bundle, and thus there is a continuous increase of temperature of both the air and the solid from one bundle to the next one. For this reason, the Nernst potential decreases, as do all of the types of losses, passing from one bundle to the next in the strip, as displayed in fig. 9b. Since the latter effect is dominant, the operating voltage (given by the Nernst voltage minus the losses) increases from bundle to bundle in the strip, as reported in fig. 9b. Fuel composition profiles are reported in fig. 9c for the third electrochemical bundle, showing a decrease of CO and H_2 and an increase of CO_2 and H_2O along the bundle, due to the electrochemical reaction. Figure 9c displays the different sources of voltage losses in the third electrochemical bundle, demonstrating that ohmic losses and losses due to the cathodic electrochemical reaction (cathodic activation) dominate under these conditions (for further information about voltage losses in the IP-SOFC concept, the reader is referred to [10]). Figure 9 reports also some results about

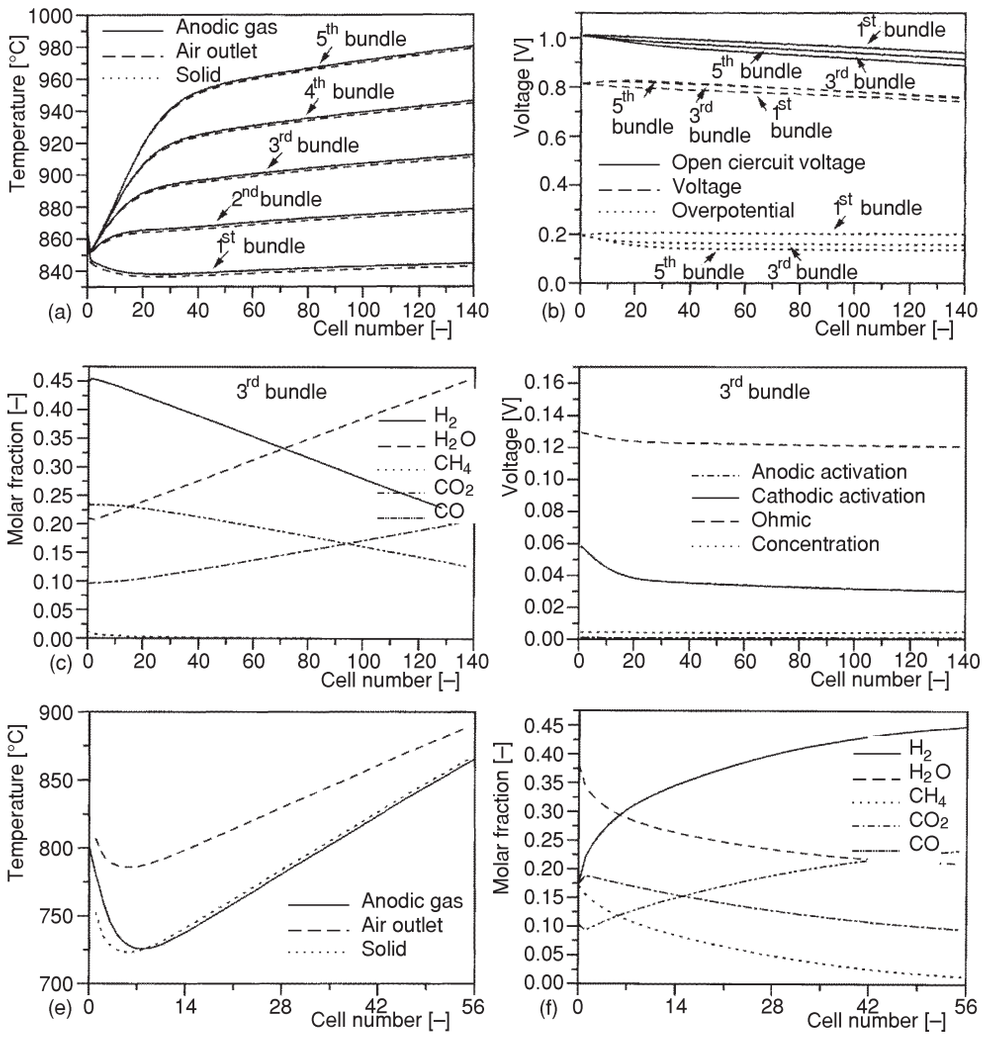

Figure 9. Simulated distributions of (a) temperatures in the electrochemical bundles, (b) electrical voltages in the electrochemical bundles, (c) fuel compositions in the 3rd electrochemical bundle, (d) voltage losses in the 3rd electrochemical bundle, (e) temperature in the reformer, (f) compositions in the reformer

the reformer. In particular, the temperature profile of the reforming bundle (fig. 9d), shows higher thermal gradients (expected to cause more significant material stresses) than in the electrochemical bundles. Figure 9d shows that in the reformer, in contrast tothe electrochemical bundles, the temperature profile of the air at the outlet of each cell is not close to the solid temperature; this is due to the fact that the air-solid heat exchange

area for the reformer (composed by 4 bundles of 14 cell equivalent modules) is much smaller than for an electrochemical bundle composed by seven 20-cell modules. Finally, the profiles of fuel composition in the reformer show a progressive increase of H_2 and CO and a decrease of CO_2, H_2O, and CH_4 content, due to the reforming and shifting reactions.

Conclusions

A modelling tool has been developed for the simulation of an IP-SOFC electrochemical reactor and a reformer; the models are based on the typical approach followed for the simulation of chemical reactors. The electrochemical reactor and the reformer have been simulated in stand-alone configuration and coupled together to form a strip, which is the fundamental repeat element of a modular plant based on the IP-SOFC technology. The simulation results are reported and discussed, as well as comparison with experimental data obtained in a narrow range of operating conditions.

Distributions of temperatures, voltages and voltage losses occurring in the electrochemical reactor are reported and discussed, as well as temperatures and compositions in the reformer. In particular, the distribution of compositions shows that strip operation is expected to be free from carbon deposition. Thermal stresses due to temperature gradients are significant only in the first module of each electrochemical bundle and in the reformer. The strip is expected to supply 1.49 kW with a predicted efficiency of 57.1%; in view of this, the IP-SOFC strip certainly represents a remarkable tool for integrated production and electrochemical conversion of H_2.

Acknowledgments

This work has been developed within the framework of the European Contracts ENK5-CT-2000-00302 and NNE5-2001-791; the authors would like to thank all the partners of those projects.

Many thanks also to Gerry Agnew, Olivier Tarnowski, Phil Butler, Robert Cunningham, and Michele Bozzolo of Rolls-Royce Fuel Cell Systems for their contribution to this work.

Nomenclature

a – thickness of gas flow duct, [m]
B – gas-solid effective heat-exchange area / cell area, [–]
c_p – specific heat, [J mol^{-1} K^{-1}]
d_h – hydraulic diameter, [m]
F – Faraday's constant, [C mol^{-1}]
h – gas-solid heat transfer coefficient, [W m^{-2} K^{-1}]
I – current density, [A m^{-2}]
K – thermal conductivity of solid, [W m^{-1} K^{-1}]

Nu – Nusselt number, [–]
n_e – number of electrons exchanged in the electrochemical reaction, [–]
n – molar flow, [mol m^{-2} s^{-1}]
p – partial pressure, [bar]
r – reaction rate, [mol m^{-3} s^{-1}]
s – solid thickness, [m]
T – temperature, [K]
V – voltage, [V]
x – co-ordinate, [m]

Greek symbols

– layer thickness, [m]
– gas heat conductivity, [W m^{-1} K^{-1}]
– stoichiometric coefficient, [–]

Subscripts

i – chemical species
g – gas
s – solid

References

[1] Rapagnà, S., Provendier, H., Petit, C., Kiennemann, A., Foscolo, P. U., Development of Catalysts Suitable for Hydrogen or Syn-Gas Production from Biomass Gasification, *Biomass & Bioenergy, 22* (2002), pp. 377-388
[2] Fuel Cell Systems (Eds. L. J. M. J. Blomen, M. N. Mugerwa), Plenum Press, NY & London, 1993
[3] Fuel Cell Handbook (5th edition), U. S. Department of Energy, Morgantown, WV, USA, 2000
[4] Magistri, L., Bozzolo, M., Tarnowski, O., Agnew, G., Massardo, A. F., Design and Off-Design Analysis of a MW Hybrid System Based on Rolls-Royce Integrated Planar SOFC; ASME Paper GT-2003-38220, *Journal of Engineering for Gas Turbines and Power,* ASME Transactions (in press)
[5] Debenedetti, P. G., Vayenas, C. G., Steady State Analysis of High Temperature Fuel Cells, *Chemical Engineering Science*, *38* (1983), pp. 1817-1829
[6] Vayenas, C. G., Debenedetti, P. G., Yentekakis, Y., Hegedus L. L., Cross-Flow Solid-State Electrochemical Reactors: A Steady-State Analysis, *Industrial & Engineering Chemistry Fundamentals, 24* (1985), pp. 316-324
[7] Achenbach, E., 3-Dimensional and Time-Dependent Simulation of a Planar Solid Oxide Fuel Cell Stack, *J. Power Sources*, *49* (1994), pp. 333-348
[8] Bessette, N. F., Wepfer, W. J., Winnick, J., A Mathematical-Model of a Solid Oxide Fuel-Cell, *Journal of the Electrochemical Society*, *142* (1995), pp. 3792-3800
[9] Costamagna, P., Honegger, K., Modeling of a Solid Oxide Heat Exchanger Integrated Stack and Simulation at High Fuel Utilization, *Journal of the Electrochemical Society*, *145* (1998), pp. 3995-4007
[10] Costamagna, P., Selimovic, A., Del Borghi, M., Agnew, G., Electrochemical Model of the Integrated Planar Solid Oxide Fuel Cell (IP-SOFC), *Chemical Engineering Journal* (in press)

[11] Bossel, U.G., Facts and Figures, final report on SOFC data, *IEA report, Operating task II*, Swiss Federal Office of Energy, Berne, CH, 1992

Authors' addresses:

P. Costamagna, F. Cerutti, R. Di Felice
DICHEP, University of Genoa,
Via Opera Pia 15, 16145 Genova, Italy
R. Collins
Rolls-Royce Fuel Cell Systems Ltd.
P. O. Box 31, Derby DE24 8BJ, UK

Corresponding author (R. Di Felice):
E-mail: difelice@dichep.unige.it

Paper submited: May 7, 2004
Paper revised: September 27, 2004
Paper accepted: October 14, 2004